One-Photon and Two-Photon Photophysical Properties of Tetrafunctionalized 5,10,15,20-tetrakis(*m*-hydroxyphenyl)chlorin (*Temoporfin*) Derivatives as Potential Two-Photon-Induced Photodynamic Therapy Agents

Piotr Gierlich,[a, b] Sebastian G. Mucha,[c] Emma Robbins,[d, e] Lígia C. Gomes-da-Silva,[b] Katarzyna Matczyszyn,*[d] and Mathias O. Senge*[f]

Photodynamic therapy (PDT) is a cancer treatment, which exploits a photosensitizing drug and light to produce reactive oxygen species that can cause selective damage to the target tissue. The second-generation photosensitizer 5,10,15,20-tetrakis(*m*-hydroxyphenyl)chlorin (*m*-THPC) is a widely used, clinically tested, and commercially available drug with the market formulation known as Foscan. *m*-THPC was used as a starting point to obtain a library of compounds with improved optical properties. Substitution, esterification and Sonogashira coupling reactions were employed to modify the *m*-THPC skeleton. Aldehyde and carboxylic acid moieties provided the possibility to enhance the two-photon absorption (TPA) cross-section while being suitable synthetic handles in the design of drug delivery systems. Characterization of their linear photophysical properties (fluorescence quantum yield, fluorescence lifetime and singlet oxygen quantum yield) was followed by the evaluation of their potential use in a non-linear absorption regime. The calculated TPA cross-section values indicate even a 2.6-fold enhancement at the TPA maximum (69.3 ± 10.0 GM), compared to *m*-THPC (26.7 ± 4.0 GM), which proves that functionalization of the *m*-THPC core leads to the improvement of the non-linear optical properties. Thus, tetrafunctionalized *m*-THPC derivatives are promising candidates for application in two-photon induced PDT.

[a] *P. Gierlich*
Medicinal Chemistry, Trinity Translational Medicine Institute
Trinity Centre for Health Sciences
Trinity College Dublin, The University of Dublin
St James's Hospital, Dublin 8 (Ireland)
[b] *P. Gierlich, Dr. L. C. Gomes-da-Silva*
CQC, Coimbra Chemistry Center
Department of Chemistry, University of Coimbra
3000-435 Coimbra (Portugal)
[c] *S. G. Mucha*
Laboratoire Charles Coulomb (L2C), UMR5221
University of Montpellier
CNRS, 34095 Montpellier (France)
[d] *E. Robbins, Prof. Dr. K. Matczyszyn*
Advanced Materials Engineering and Modelling Group
Faculty of Chemistry
Wroclaw University of Science and Technology
Wyb. Wyspianskiego 27, 50-370 Wroclaw (Poland)
E-mail: katarzyna.matczyszyn@pwr.edu.pl
[e] *E. Robbins*
Faculté des Sciences et Techniques
Université de Limoges, PEIRENE, EA 7500
123 Avenue Albert Thomas, CEDEX, 87060 Limoges (France)
[f] *Prof. Dr. M. O. Senge*
Institute for Advanced Study (TUM-IAS)
Technical University of Munich
Lichtenbergstrasse 2a, 85748 Garching (Germany)
E-mail: mathias.senge@tum.de
Homepage: http://www.sengegroup.eu/

Supporting information for this article is available on the WWW under https://doi.org/10.1002/cptc.202100249

Introduction

Photodynamic therapy (PDT) is a minimally invasive anti-cancer treatment method, which uses the combined effect of a photosensitizing drug, light, and oxygen to cause selective damage to the target tissue.[1] The fundamental concept behind PDT involves the administration of a photosensitizing agent (pro-drug) and subsequent photoactivation by light of a specific wavelength to act against the target cells. Over the last three decades, PDT has been used in clinical practice to treat solid tumors.[2]

A photosensitizer (PS) is a chromophore that, upon photoexcitation, has the ability to efficiently produce the triplet excited state and react with oxygen or biomolecules to produce highly toxic reactive oxygen species (ROS). The photophysical processes taking place during PDT are illustrated in Scheme 1. Initially, the PS is in the ground electronic singlet state (S_0) and, after irradiation with light of a suitable wavelength absorbed by the molecule in a one-photon or two-photon process, it is excited to a singlet state (S_1). The return to the ground S_0 state is possible by emitting the absorbed energy as fluorescence (used for diagnostics and imaging) or through radiationless decay. Alternatively, the S_1 state can undergo intersystem crossing (ISC) to the excited triplet state (T_1). The efficiency of ISC depends on a number of factors, including so-called spin-orbit coupling. Because the radiative transition from T_1 to S_0 (phosphorescence) is spin forbidden, the T_1-state is often long-lived, so it can take part in different chemical

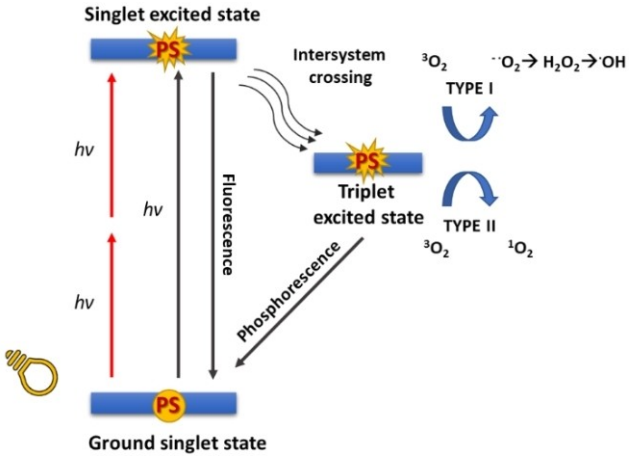

Scheme 1. Schematic representation of one-photon and two-photon (in red) excitation processes.

reactions. Alternatively, the PS can return to the S_0-state *via* radiationless decay.[3,4]

As indicated in Scheme 1 the excitation of the chromophore can occur not only by the usual one-photon absorption (OPA), but also by a two-photon process where two lower energy photons, with equal transition energy are simultaneously absorbed. While the dependence of the rate of generation of the excited state on the light intensity is linear in one-photon processes, it is quadratic for the two-photon processes, requiring short-pulse lasers for activation of the molecule.[5] To overcome drawbacks of conventional PDT, development of new drug delivery systems (DDS)[6] (hydrogels,[7,8] inorganic nanoparticles[9–12]) combining advances of TPA and nanotechnology, opens promising possibilities to improve treatment efficacy. This approach allows for better tumor targeting, excitation of chromophores at longer laser wavelengths and deeper tissue penetration.[13]

The crucial factor that determines suitability of a photosensitizer for use in two-photon PDT is its TPA cross-section. This quantity can be determined experimentally by Z-scan and Two-Photon Excited Fluorescence (TPEF). While Z-scan is based on the measurement of light intensity as the function of the sample position along the z-axis, the TPEF technique investigates the intensity of the two-photon induced fluorescence as the function of the excitation intensity. However, both techniques have their limitations. When using the Z-scan technique, the TPA cross-section values tend to be more enhanced compared with other techniques, which often correlates with the presence of non-linear scattering or defocusing of the sample during the measurements. In turn, TPFE can only be applied for fluorescent molecules and cannot overlap with the one-photon absorption regions. In the case of species with a reasonably high luminescence quantum yield, using TPEF is usually preferred. Typically, the experiment is carried out by comparing the signal from an investigated sample with that from a reference fluorescent dye, avoiding the need for exact knowledge of variables dependent on the laser beam.[14]

The desired properties of photosensitizers for two-photon excited (TPE) PDT have been extensively reviewed in the literature.[15,16] Various synthetic strategies to improve the TPA cross-section values of a PS is the introduction of conjugated systems, donor or acceptor moieties and enhancement of molecular coplanarity.[17,18,19] Generally, large enhancements can be obtained by the increase of the size of the π-electron system and the distance of a donor (HOMO) to an acceptor (LUMO) moiety.[20,21] Moreover, increasing the electronic and hole density motifs within the molecule in the first singlet excited state can lead to the enhancement of the TPA cross-section values. This can be quantified by the Δr index which determines the distance of the intramolecular charge transfer.[22]

5,10,15,20-Tetra(*m*-hydroxyphenyl)chlorin (*m*-THPC) is a second generation PS with the generic name *temoporfin* and is clinically registered as the drug formulation Foscan®.[23,24] This molecule belongs to the family of reduced porphyrins and was synthesized by Bonnett *et al.* over three decades ago.[25] The properties of *m*-THPC include strong absorption at 650 nm and good chemical stability. Additionally, Foscan® is approved in the European Union for the palliative treatment of head and neck cancer.[26] Nonetheless, *m*-THPC has several limitations such as limited solubility in aqueous media, leading to photosensitizer aggregation, non-specific accumulation, and prolonged skin photosensitivity. PDT as a continuously developing cancer treatment method, constantly requires further modifications of the PS to improve treatment efficacy. Several modifications such as conjugation with anti-inflammatory drugs,[27] bioconjugation with targeting ligands,[28,29] and incorporation into nanoformulations have been reported.[30,31]

Herein, *m*-THPC was used as a starting point to obtain derivatives aimed at overcoming the PS's limitations. Synthetic procedures such as substitution, esterification, and Sonogashira coupling reactions were employed to modify the *m*-THPC skeleton providing aldehyde and carboxylic acid moieties aiming to enhance the TPA cross-section, while being suitable synthetic handles in the design of DDS, and to improve the therapeutic effect. Linear photophysical parameters including fluorescence quantum yield (FLQY), fluorescence lifetime and singlet oxygen quantum yield were evaluated. Furthermore, the TPA cross-section values of *m*-THPC derivatives were determined using the TPEF technique, which confirmed their potential application in two-photon induced PDT.

Results and Discussion

Synthesis and Characterization of *m*-THPC Derivatives

Our interest to implement synthetic modifications of *m*-THPC arose in order to design novel DDS overcoming current limitations related to Foscan.[32] To achieve that goal, simple *m*-THPC functionalization reactions were performed, providing aldehyde and carboxylic moieties, useful for many synthetic strategies in the design of novel platforms for drug delivery (Scheme 2). Moreover, due to the previously reported ability of

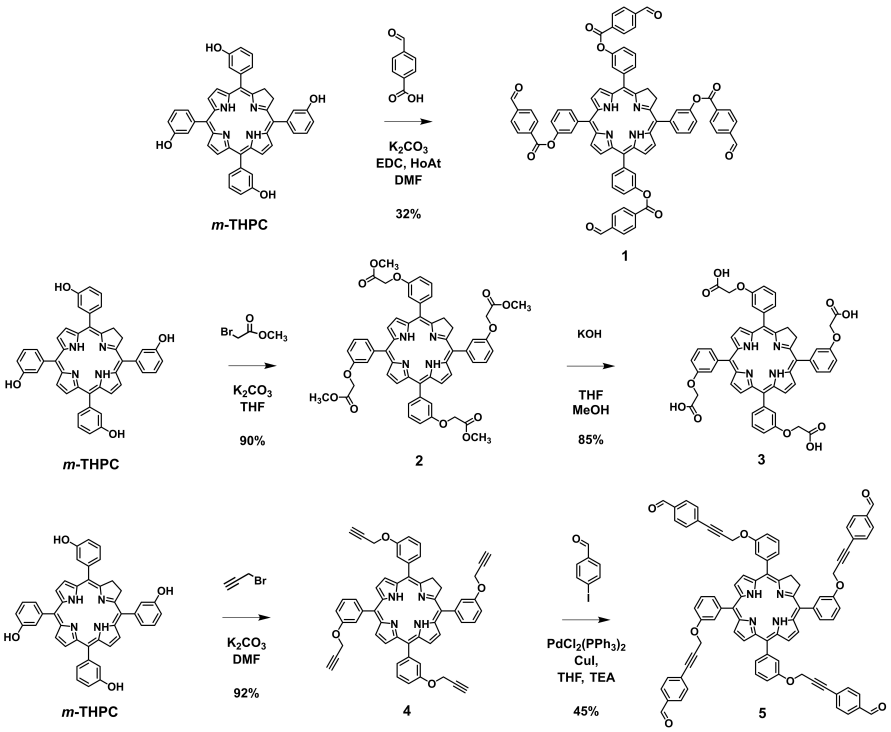

Scheme 2. Synthesis of tetrafunctionalized *m*-THPC derivatives.

m-THPC to perform TPE PDT,[33] we surmised that the introduced modifications will have a positive impact on the TPA cross-section values, opening the door for potential application as TPE PDT dyes.

Tetrafunctionalizations of the *m*-THPC system were performed applying cost-efficient, reliable chemistry procedures. The PS **1** was obtained following the procedure previously described by Rogers *et al. via* a one pot esterification reaction.[27] Water soluble 1-ethyl-3-(3-dimethylaminopropyl)carbodiimide (EDC) hydrochloride and 1-hydroxy-7-azabenzotriazole (HOAt) were used to activate the carboxylic acid groups of 4-carboxybenzaldehye at the same time allowing for easy removal during the reaction workup. HOAt was used to reduce the suppressive activity of the EDC side product, *N*-acylurea, allowing for a better reaction efficiency. The reaction gave the desired product **1** in 32% yield but provided other derivatives with a different degree of substitution in the reaction mixture. The tetrafunctionalized product exhibited the highest retention factor (R_f) on thin-layer chromatography and monosubstituted the lowest.

Molecule **3**, containing carboxylic acid moieties, was synthesized in a two-step procedure. First, the hydroxyl groups of the *m*-THPC skeleton were modified in a nucleophilic substitution reaction with methyl bromoacetate, resulting in the formation of compound **2** with 90% reaction yield. Next, the intermediate containing ester groups was hydrolyzed using potassium hydroxide, leading to precipitation of the final product (85% yield).

Derivative **5** was synthesized in a two-step synthetic procedure. The first step was the nucleophilic substitution of the hydroxyl group of *m*-THPC with propargyl bromide applying the conditions described by Rogers *et al.*[34] Compound **4** was obtained in a 92% yield, and next, the propargyl groups were reacted with aryl halide – 4-iodobenzaldeyde *via* Sonogashira coupling reaction. The coupling reaction was carried out at 45 °C in dry tetrahydrofuran (THF) in the presence of copper (CuI) and palladium (bis(triphenylphosphine)palladium (II) dichloride) catalysts to promote reaction with terminal alkynes that next undergo an oxidative addition followed by reductive elimination to form product **5** in a 45% yield.

The *m*-THPC derivatives were characterized using 1D NMR spectroscopy, MALDI-TOF mass spectrometry (MS), UV/Vis and fluorescence spectroscopy. The NMR spectra recorded in deuterated chloroform ($CDCl_3$) for PS **1**, **5** and deuterated dimethyl sulfoxide (DMSO-d_6) for PS **3**, respectively and MS data are included in the Supporting Information (SI) (Figures S1–S21). The ^{1}H NMR spectra of compounds **1**, **3** and **5** are consistent with the structure of *m*-THPC which was originally evaluated in detail by Bonnett *et al.*[35] Hydrogen atoms on the reduced pyrrole ring, characteristic for chlorins, appear as a singlet at 4.15–4.25 ppm, and the NH protons of the macrocycle with a singlet at −1.5 to 1.6 ppm. Moreover, the NMR spectra of the derivatives contain characteristic signals for the functional groups – aldehyde for **1** and **5** at 10.12 and 10.08–9.88 ppm, respectively. However, the carboxylic signal of **3** recorded in DMSO-d_6 is not visible in the spectrum due to peak broadening. Furthermore, the synthesis of *m*-THPC derivatives and reaction intermediates were confirmed by MS.

Absorption, Excitation, and Emission Properties

The absorption, excitation, and emission spectra were measured in order to provide a comparative evaluation of their linear photophysical properties. No significant differences between the derivatives were observed in the positions of the Soret and Q bands, remaining in the range 420 to 422 nm and 651 to 653 nm, respectively, confirming data reported in the literature for the spectral properties of *m*-THPC. As expected, the absorption and excitation spectra recorded at 650 nm overlap each other (Figure 1A, S22–24). Furthermore, the red fluorescence spectrum of each PS was found to exhibit a sharp emission peak at 650 nm, with the full-width half-maximum (FWHM) values estimated to be *ca.* 18 nm, upon excitation in the wide wavelength range from the near-ultraviolet (NUV) and visible regions. However, the compounds differed in the emission efficiency. The strongest red emission signal appeared upon excitation at 420 nm corresponding to the absorption maximum of the Soret band (Figure S25).

The concentration-dependent aggregation-induced fluorescence quenching of macrocyclic molecules is a common phenomenon occurring due to the increased interactions between the same molecules, in comparison with the interactions with a solvent. This phenomenon for *m*-THPC in methanol solution was previously described by Bonnet *et al.*[26] Moreover, the absolute fluorescence quantum yields (FLQY) and ability to generate singlet oxygen ($^1O_2$) is strongly affected by this process, leading to a decrease of the phototoxic activity of the compound.[36] We observed that for dimethylformamide (DMF) solutions of *m*-THPC the strongest fluorescence intensity signal was observed at the concentration of 10 μM, while for derivatives **1**, **3** and **5** it was at 8 μM. With increasing concentration of the PSs, a gradual decrease of fluorescence intensity was observed (Figure 1B). Additionally, with increasing concentration of the PS the emission band at 652 nm, present in the non-aggregated form, was broadened, and shifted towards the red part of the spectrum resulting in fluorescence maxima of 662 nm for *m*-THPC, 663 nm for **3**, and **5** and 664 nm for **1** (Figure S26). These spectral red-shifts that arise from an aggregation process are typical for the self-organization of organic dyes with dominating planar cores.[37]

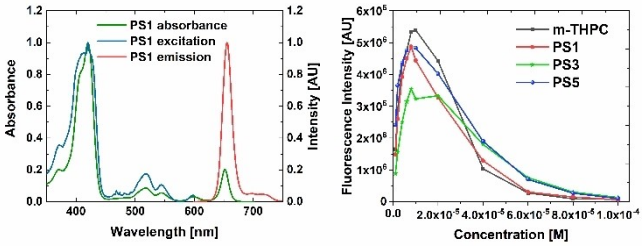

Figure 1. Left) Normalized UV/Vis absorption spectra, excitation spectra (for 650 nm emission wavelength) and emission spectra (for the 420 nm excitation wavelength) of PS **1** in air-saturated DMF at the concentration of 10^{-6} M. Right) Dependence of fluorescence intensity (at 650 nm) on concentration in DMF for *m*-THPC, PS **1**, **3** and **5**.

Fluorescence Quantum Yields, Fluorescence Decay Times and Radiative and Nonradiative Constants

FLQYs measured in DMF were calculated to be $\phi_f \approx 44.1\,\%$, 39.5 %, 38.1 % and 24.6 % for *m*-THPC, PS **1**, **3**, and **5**, respectively. Fluorescence of *m*-THPC and tetrafunctionalized derivatives were found to be enhanced in DMF in comparison to more polar solvents such as DMSO, or as previously reported in ethanol (QY = 8.9 %).[38] To our knowledge there is no FLQY data of *m*-THPC reported in DMF. Although the difference between fluorescence intensity of *m*-THPC and derivatives **1** and **3** is not significant, a decrease of over 20 % of the emission intensity was observed for PS **5**. This decreased fluorescence intensity may be due to the reduced rigidity of the corresponding molecular structure. Moreover, this is reflected in the increased value of the non-radiative constant (k_{nr}) (0.089 ns^{-1}) for PS **5** in comparison with other derivatives (0.059–0.067 ns^{-1}).[12] The fluorescence decays of the *m*-THPC derivatives were recorded at 650 nm using time-correlated single-photon counting technique (TCSPC). The obtained decay curves were fitted using mono (*m*-THPC, PS **1**, PS **3**) or bi-exponential (PS **5**) functions (Figure 2).

Fluorescence lifetime values of *m*-THPC, PS **1**, and **3** were found to be in the range from 9.2 to 9.3 ns (Table 1), while PS **5** reveals two fluorescence lifetime components, denoted as T_1 and T_2, respectively. Although the T_2 component reaches a similar value to other derivatives (9.51 ns), the T_1 value was slightly lower (6.25 ns), and therefore, the as-calculated intensity-weighted average value was estimated to be 8.50 ns (Table 2). The fluorescence lifetime τ depends on the intrinsic characteristics of the fluorophore itself and on the local environment. Collected data of FLQY and long fluorescence lifetimes allowed for a calculation of radiative (k_r) and non-radiative rate constants (Table 1). The ratio of k_{nr} to k_r indicates the predominance of non-radiative over radiative processes.

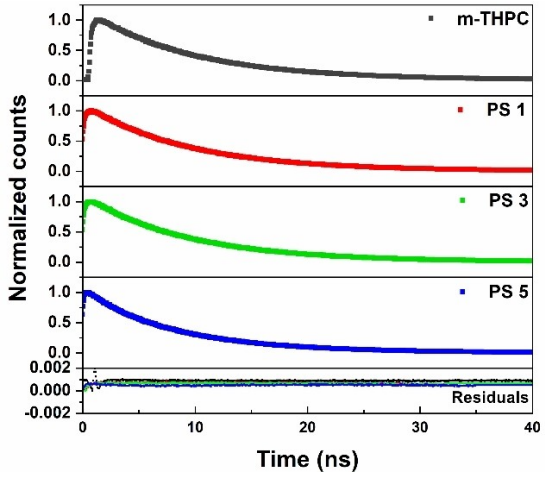

Figure 2. Fluorescence decay of *m*-THPC and *m*-THPC derivatives **1**, **3** and **5**, after excitation at 377 nm in air-saturated DMF solution.

Table 1. Fluorescence quantum yields, fluorescence decay times (τ) and radiative and non-radiative constants of *m*-THPC and tetrafunctionalized *m*-THPC derivatives **1**, **3** and **5**. (SE = standard error).

PS	FLQY [%]	SE of FLQY [%]	Average τ [ns]	k_r [ns^{-1}]	k_{nr} [ns^{-1}]
***m*-THPC**	44.1	3.9	9.31	0.048	0.059
PS1	39.5	1.4	9.26	0.043	0.065
PS3	38.1	1.5	9.24	0.041	0.067
PS5	24.6	1.5	8.50	0.029	0.089

Table 2. Fluorescence lifetime parameters of PS **5**: Lifetime components (T_1 and T_2) and amplitude values (A_1 and A_2).

PS	T_1 [ns]	A_1 [%]	T_2 [ns]	A_2 [%]	Average τ [ns]
PS 5	6.25	40.5	9.51	59.5	8.50

Singlet Oxygen Quantum Yield

The results indicate that there are no significant differences in $^1O_2$ generation efficiencies between the derivatives **1**, **3**, **5** and *m*-THPC, being in the range from 25% to 31% when quantified in DMSO (Table 3). Slightly larger differences could be noted for the values determined in DMF, varying in the range from 64%, for the hydrophilic PS **3**, to 76% for hydrophobic derivative **1**. The difference between $^1O_2$ quantum yields calculated in both solvents is attributed to quenching processes occurring in different solvents with $^1O_2$. This phenomenon has been extensively elaborated by Ogilby *et al.*[39] Nevertheless, it can be concluded that the expansion of the *m*-THPC skeleton does not negatively impact its photophysical properties. Obtained experimental values of the $^1O_2$ quantum yield of *m*-THPC in both solvents corresponds with the literature data (68% in DMF and 40% in DMSO)[40,41] whereas small discrepancies are within the experimental error.

The lifetime of $^1O_2$ is dependent on the properties of the solvent and related with different kinetics of the energy transfer from $^1O_2$ in a given system, defined as a solvent quenching constant. The average lifetime of $^1O_2$ was calculated for both DMF and DMSO (Figure 3, Table 3) and compared to literature values. For DMF, the calculated average value of 20 μs stays in line with previously obtained values (18.9 and 14 μs).[42,43]

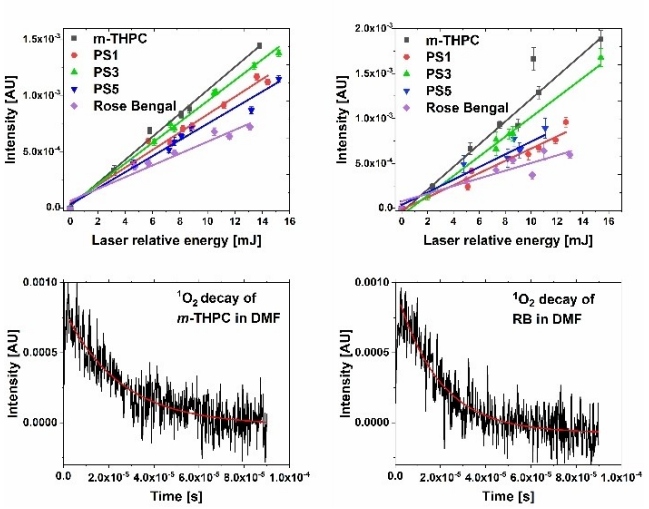

Figure 3. $^1O_2$ phosphorescence intensities in DMF (top left) and DMSO (top right) as a function of the laser pulse energy. Representative $^1O_2$ phosphorescence decays of *m*-THPC (bottom left) and Rose Bengal (bottom right) recorded in DMF.

An analogous situation was observed in DMSO, resulting in average lifetimes in a range of 6.9–9.6 μs which corresponds with the literature value of 5.6 μs.[44,45] However, other reported values for DMSO can be found ranging up to 19 μs.[46] These discrepancies between $^1O_2$ lifetimes were extensively discussed by Oelckers *et al.* and they might be caused by factors such as different measurement methods, apparatus sensitivity, solvent quality, temperature, or light source potency.[47] Nonetheless, the discrepancies of $^1O_2$ lifetimes between *m*-THPC and tetrafunctionalized derivatives PS **1**, **3** and **5** are in the range of available literature data.

Table 3. $^1O_2$ quantum yield (Φ_Δ) and $^1O_2$ lifetime (τ) data for *m*-THPC and tetrafunctionalized derivatives PS **1**, **3** and **5** in DMSO and DMF. (SE = standard error).

PS DMSO	Mean $^1O_2$ τ [s]	SE of mean	Φ_Δ [%]	Se of mean [%]
***m*-THPC**	8.62E-06	2.16E-06	**29.8**	6.9
PS1	9.68E-06	7.64E-07	**26.1**	3.4
PS3	6.96E-06	4.31E-07	**30.8**	5.6
PS5	7.81E-06	1.50E-06	**24.6**	4.4
Rose Bengal	8.00E-06	1.58E-06	**16.0**	–
DMF				
***m*-THPC**	1.91E-05	1.13E-06	**73.8**	3.7
PS1	2.04E-05	1.77E-06	**76.0**	2.4
PS3	2.02E-05	1.42E-06	**64.1**	4.6
PS5	2.03E-05	6.62E-07	**67.7**	4.6
Rose Bengal	2.05E-05	9.44E-07	**47.0**	–

Nonlinear Properties of m-THPC and Tetrafunctionalized Derivatives

Two-Photon Absorption and Two-Photon Excited Emission Spectra

All *m*-THPC derivatives exhibited an intense emission upon femtosecond laser irradiation in the NIR region (Figure 4 and S27). As in previous cases,[48–50] power dependence measurements of emission intensities were performed ($\lambda_{exc.}$ = 840 nm). The corresponding logarithmic plot of emission intensity *vs.* input power is shown in Figure S28 with a slope value of 1.87 indicative of quadratic power relation, and confirming the TPA process. Similar tendencies were previously noticed for *m*-THPC

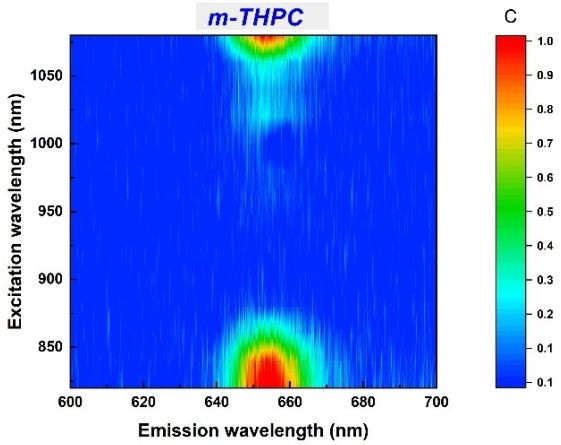

Figure 4. The TPE excitation-emission map of *m*-THPC in DMF. The relative molar concentration was adjusted so the corresponding absorbance value was kept below 0.1 in the emission region.

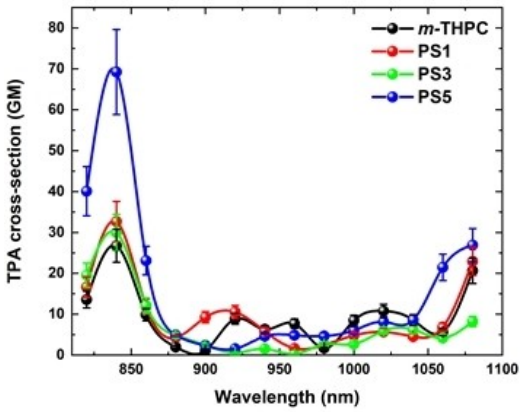

Figure 5. TPA spectra of all compounds in DMF. The relative molar concentration were adjusted allowing the corresponding absorbance value being kept below 0.1 in the emission region.

and its macromolecular modifications.[48,52] Both one-photon excited (OPE) and TPE fluorescence spectra of all compounds in DMF solution cover the red color range ($\lambda_{max.}$ = 655 nm) with the narrow emission profiles *i.e.*, high color purity. To gain a deeper insight into the TPA properties of our compounds, TPA cross-section values (σ_{TPA}) were estimated by TPE emission measurements (Figure 5). σ_{TPA} values were determined with respect to the commercially available dye **LDS-698**, in chloroform.[53] The most representative parameters at the TPA maxima are displayed in Table 4.

The OPA and TPA spectra of *m*-THPC and other derivatives are compared in Figure 6 and S29. As expected, there is a good overlap of the major TPA peak with double the wavelength of the Soret band (at 840 nm and 420 nm, respectively). Considering their very similar spectral behavior and the non-centrosymmetric design, it is evidenced that OPA and TPA may reach the same excited state. The small red-shift in the TPA spectra corresponds with the possible, partial, re-absorption of the emission occurring during the OPA processes, which is related to the different penetration depths of the light beam.[54] Additionally, the compounds feature weaker TPA (~10–20 GM) in the longer wavelength region (>1000 nm) which are related to Q-bands from one-photon transitions.

Among all *m*-THPC derivatives, the TPA cross-section values follow the trend PS **5** > PS **1** > PS **3** > *m*-THPC (Figure 5, Table 4). It is well-known that extending the π-conjugation length of a molecule generally leads to an enhancement of the TPA cross-section.[7,9,55] This was observed with the change from carbonyl (PS **1**) to alkyne linkers (PS **5**), and the significant increase in the TPA cross-section value. Considering the literature reports, direct meso-substitution of the functional groups to the porphyrin core has shown to have an efficient enhancement of both the TPA cross-section and brightness, despite hindering conjugation.[56]

With the electron accepting groups at the end of the molecules (PS **1**, PS **3**, and PS **5**), in a donor-acceptor (D-A) motif, the extent of charge transfer from the center of the molecule is also increased. The observed difference in the TPA cross-sections is most likely due to the difference in the strengths of the electron-accepting end groups (ketone in PS **1** and PS **5** being more strongly electron-accepting than the carboxylic acid group in PS **3**). It has been reported that a simpler molecular configuration, such as the D-A architecture of PS **1**, **3**, and **5**, leads not only to a significant enhancement of the TPA cross-section, but to increased brightness as well.[57] With these simple modifications we have managed to improve the TPA activity, indicating even a 2.6-fold enhancement at the TPA maximum of PS **5** (69.3 ± 10.0 GM), compared to *m*-THPC (26.7 ± 4.0 GM). Varying molecular structures also induces different TPA peaks at double the wavelength of the Q-band regions (Figure 6 and S29).

Although *m*-THPC and its derivatives are known as strong emitters and superior photosensitizers, their multiphoton-excited fluorescence and multiphoton absorption features have only found limited attention. Hamed *et al.* reported the TPA spectrum in the Q-band transition regime (1050–1450 nm) and around the Soret band using the open aperture Z-scan technique. TPA cross-sections of *m*-THPC in DMSO were measured to be around 20 GM at 1320 nm and 28 GM at 775 nm,[33] also showing similar spectral behavior in OPA and TPA spectra. Furthermore, TPE fluorescence at a single excitation wavelength (800 nm) has been previously reported for *m*-THPC in a solvent mixture (20% ethanol, 30% polyethylene glycol, and 50% distilled water) to be 18 GM.[51]

Table 4. Non-linear optics parameters of *m*-THPC and derivatives in DMF ($\lambda_{exc.}$ = 840 nm).

PS	σ_{TPA} [GM]	Normalized σ_{TPA} [GM/Da]	Brightness [$\varphi^{\bullet}\sigma_{TPA}$]
***m*-THPC**	26.7 ± 4.0	0.039	12.0
PS1	32.7 ± 4.9	0.048	12.9
PS3	30.0 ± 4.5	0.033	11.4
PS5	69.3 ± 10.0	0.056	17.0

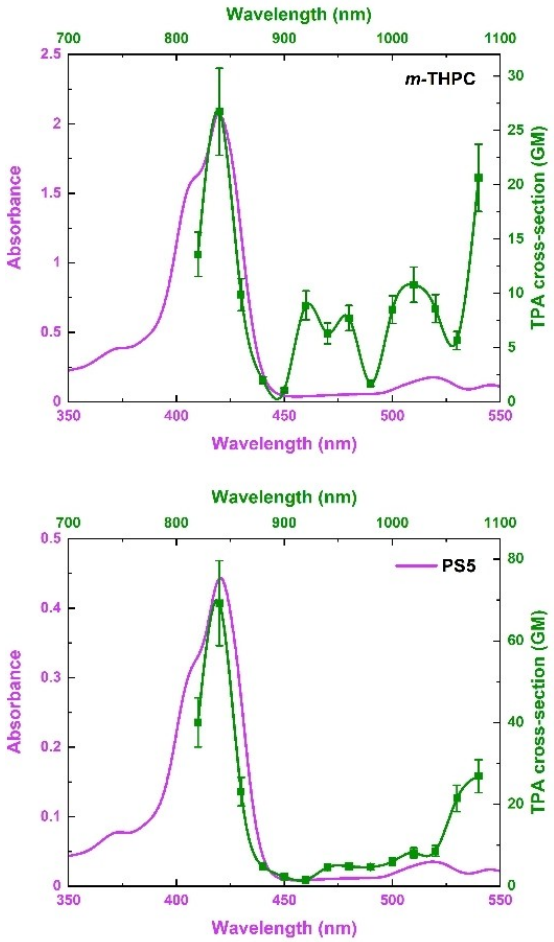

Figure 6. OPA (pink) and TPA (green) spectra of *m*-THPC (top) and PS **5** (bottom) in DMF. The relative molar concentrations were adjusted allowing the corresponding absorbance value being kept below 0.1 in the emission region.

Transfer to Aqueous Solution and Nonlinear Optic Properties

The intense red fluorescence produced upon two-photon excitation lying in the first biological optical window gives promise for the use of these compounds as TPE-fluorescence imaging agents. As expected, attaching carboxyl groups to meso-phenyl rings allows PS **3** to be dissolved in water with no pre-treatment process. Importantly, although the transfer to an aqueous medium does not quench TPE fluorescence, spectral differences are observed. Figure 7 shows that the red-shifted emission (~670 nm) component plays a more crucial role in buffer solution rather than the blue-shifted one (~655 nm) that dominates in DMF solutions. This may indicate the significant contribution of H-like agglomerates to TPE fluorescence. Nevertheless, the existence of strong TPE red fluorescence at stimulated physiological conditions indicates the potential of PS **3** in biomedical applications.

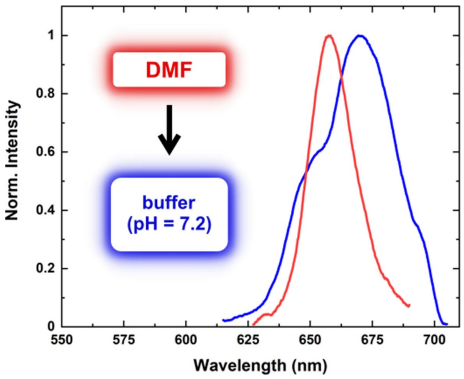

Figure 7. Transfer from DMF to buffer (pH = 7.2) effect on TPE fluorescence spectra of PS **3**.

Conclusions

We reported convenient synthetic procedures introducing aldehyde and carboxylic groups to the skeleton of *m*-THPC, and investigated the photophysical effects of modifying the *m*-THPC structure. Quantifying $^1O_2$ generation efficiency and fluorescence properties of derivatives, we found that introduction of peripheral functional groups does not have a significant effect on their properties in comparison to the mother compound. The non-linear properties of *m*-THPC and derivatives were investigated using two-photon excited fluorescence in DMF, showing that simple modifications of the *m*-THPC skeleton increase the TPA activities. This was proven by determination of the two-photon cross-section, indicating a 2.6-fold enhancement at the TPA maximum for PS **5**, containing alkyne linkers between the *m*-THPC core and the introduced carbonyl groups.

Moreover, the existence of fluorescence in aqueous media of PS **3** after two-photon excitation opens a door to explore its properties as fluorescence imaging probes. Future work will, in addition to *in vitro* and *in vivo* studies, include development of systems aiming to use the combined effect of the non-linear properties of the compounds described here, together with nanoformulation strategies for application in two-photon induced PDT.[58] It is hoped that the development of DDS using *m*-THPC derivatives as *cross-linkers* in polymeric nanoparticles will allow for the excitation of chromophores at longer laser wavelengths, leading to deeper penetration of the treated tissues, and in consequence, better therapeutic response and reduction of side effects related to Foscan treatment.

Experimental Section

Materials

General Information and Instrumentation are provided in the Supporting Information.

Synthesis of 5,10,15,20-Tetrakis[3-(4-formylbenzoate)phenyl]chlorin (1). *m*-THPC (200 mg, 0.29 mmol.), K_2CO_3 (487 mg, 3.53 mmol.), HOAt (479 mg, 3.53 mmol.), EDC

hydrochloride (676 mg, 3.53 mmol.), and 4-formylbenzoic acid (529 mg, 3.53 mmol) were added to a Schlenk flask. The reagents were stirred and dried under vacuum for 1 hour. Dry DMF (10 mL) was added to the flask and the reaction was stirred for 20 hours under argon. The reaction was monitored by TLC. When full conversion of the starting material was observed, the reaction was terminated by the addition of CH_2Cl_2 (50 mL). The reaction mixture was washed using distilled water (2×30 mL), $NaHCO_3$ (2×30 mL), NaCl (2×30 mL), and distilled water (2×30 mL). The organic phase was evaporated under reduced pressure. The product was purified on a silica gel column using CH_2Cl_2/n-hexane/methanol (3:1:0.1) as the eluent. The first purple band was collected and evaporated under reduced pressure and then recrystallized (CH_2Cl_2:hexane). The products were isolated as a purple solid (112 mg, 0.092 mmol, 32%). M.p. > 250 °C; R_f = 0.46 (SiO_2, CH_2Cl_2:hexane:methanol – 3:1:0.1); ^{1}H NMR (400 MHz, chloroform-*d*) δ 10.12 (s, 4H, CHO), 8.73 (d, *J* = 4.9 Hz, 2H, H_β), 8.56 (s, 2H, H_β), 8.42 (d, *J* = 3.6 Hz, 8H, Ar–H), 8.34 (d, *J* = 4.9 Hz, 2H, H_β), 8.10–7.95 (m, 12H, Ar–H), 7.79 (m, 8H, Ar–H), 7.63 (dd, *J* = 8.1, 1.6 Hz, 2H, Ar–H), 7.57 (dd, *J* = 8.1 Hz, 2H, Ar–H), 4.36–4.20 (s, 4H, H_β), −1.50 (s, 2H, N–H) ppm; ^{13}C NMR (101 MHz, chloroform-*d*) δ = 191.42, 167.52, 164.32, 152.35, 150.44, 149.37, 144.37, 143.48, 140.58, 139.53, 135.09, 131.91, 130.72, 129.58, 127.87, 121.48, 111.38, 65.32, 42.00, 30.16, 29.15, 23.37, 23.12, 14.13, 11.13, 1.07 ppm; UV/Vis (chloroform): λ_{max} (log ε) = 421 (5.31), 519 (4.19), 547 (3.99), 601 (3.77), 654 nm (4.57); HRMS (MALDI) *m/z* calcd. for $C_{76}H_{48}N_4O_{12}$ $[M]^+$: 1208.3269, found 1208.3257; IR (ATR): $\tilde{\nu}$ 1979.5, 1734.2, 1701.4, 1602.9, 1575.8, 1470.7, 1419.2, 1382.6, 1301.5, 1245.2, 1198.1, 1149.0, 1066.4, 1018.8, 100.2, 944.0, 918.8, 778.3, 750.6, 721.5, 681.1, 629.1 cm^{-1}.

Synthesis of 5,10,15,20-Tetrakis[3-(1-propan-2-one)phenyl]chlorin (2). *m*-THPC (200 mg, 0.29 mmol.) and Cs_2CO_3 (449 mg, 2.94 mmol.) were weighted out and added to a Schlenk flask. The reagents were dried under vacuum for 1 hour. Dry DMF (10 mL) was added to the flask and the reaction was stirred for 15 minutes. Next, methyl bromoacetate (957 mg, 2.94 mmol.) was added and the reaction mixture was stirred for 20 hours at 45 °C under an argon atmosphere. The reaction was monitored by TLC. When full conversion of the starting material was observed, the reaction was terminated with the addition of CH_2Cl_2 (50 mL). The reaction mixture was washed using distilled water (2×30 mL), $NaHCO_3$ (2×30 mL), and NaCl (2×30 mL). The organic phase was evaporated under reduced pressure. The product was purified on silica gel column using CH_2Cl_2/n-hexane/methanol (3:1:0.1) as the eluent. The first purple band collected was evaporated under reduced pressure and recrystallized (CH_2Cl_2:hexane). The product was isolated as a purple solid (250 mg, 0.27 mmol, 90%). M.p.: > 300 °C; R_f = 0.6 (SiO_2, CH_2Cl_2:hexane:methanol – 3:1:0.2); ^{1}H NMR (400 MHz, chloroform-*d*) δ 8.59 (d, *J* = 4.9 Hz, 2H, H_β), 8.43 (s, 2H, H_β), 8.20 (d, *J* = 4.8 Hz, 2H, H_β), 7.75 (d, *J* = 7.6 Hz, 2H, Ar–H), 7.65 (s, 2H, Ar–H), 7.60 (q, *J* = 6.9 Hz, 4H, Ar–H), 7.51 (d, *J* = 7.4 Hz, 2H, Ar–H), 7.43 (s, 2H, Ar–H), 7.30 (dd, *J* = 8.4, 2.1 Hz, 2H, Ar–H), 7.23 (dd, *J* = 8.4 Hz, 2H, Ar–H), 4.79 (m, 8H, CH_2), 4.17 (s, 4H, H_β), 3.80 (s, 12H, CH_3), −1.51 (s, 2H, N–H) ppm; ^{13}C NMR (101 MHz, chloroform-*d*) δ 169.33, 169.31, 167.12, 157.41, 156.23, 152.21, 144.37, 143.43, 140.47, 134.94, 131.92, 129.13, 128.00, 127.87, 127.69, 126.04, 123.40, 121.96, 120.15, 118.69, 114.35, 113.88, 111.74, 65.47, 63.72, 57.91, 52.27, 35.60 ppm; UV/Vis (chloroform): λ_{max} (log ε) = 420 (5.39), 519 (4.26), 547 (4.06), 600 (3.86), 654 nm (4.65); HRMS (MALDI) *m/z* calcd. for $C_{56}H_{48}N_4O_{12}$ $[M]^+$: 968.3269, found 968.3258;

Synthesis of 5,10,15,20-Tetrakis[3-(acetic acid)phenyl]chlorin (3). *m*-THPC derivative **2** (200 mg, 0.22 mmol.) was weighted out and added to a Schlenk flask. The reagents were dried under vacuum for 1 hour. THF (5 mL) and methanol (5 mL) were added to the flask and the reaction mixture was stirred for 15 min at room temperature. Next, KOH (148 mg, 2.63 mmol.) dissolved in distilled water (2 mL) was added to the flask and the reaction mixture was stirred overnight under reflux (80 °C). The reaction was monitored by TLC and, after full conversion, terminated. The solvent was evaporated, and distilled water (3 mL) was added to the reaction mixture. Next, the crude product was neutralized with an appropriate amount of 2 M HCl solution. The product was filtered using on a Büchner flask using and dried. The product was isolated as a purple solid (172 mg, 0.18 mmol, 85%). M.p. > 300 °C, ^{1}H NMR (400 MHz, dimethyl sulfoxide-d_6) δ 8.62 (d, *J* = 4.7 Hz, 2H, H_β), 8.36 (s, 2H, H_β), 8.22 (d, *J* = 4.8 Hz, 2H, H_β), 7.66 (d, *J* = 6.2 Hz, 4H, Ar–H), 7.63 (s, 2H, Ar–H), 7.47 (m, 4H, Ar–H), 7.32 (dd, *J* = 7.2 Hz, 2H, Ar–H), 7.25 (dd, *J* = 8.6 Hz, 2H), 4.84 (m, *J* = 11.0 Hz, 8H, CH_2), 4.16 (s, *J* = 29.3, 13.8 Hz, 4H, H_β), −1.63 (s, 2H, N–H) ppm; ^{13}C NMR (101 MHz, methanol-d_4) δ 171.58, 157.91, 156.98, 143.56, 142.46, 135.36, 128.89, 128.25, 127.76, 125.25, 123.90, 121.23, 120.75, 118.51, 114.27, 113.78, 113.05, 64.79, 38.97, 35.27 ppm; UV/Vis (methanol): λ_{max} (log ε) = 418 (5.18), 518 (4.10), 545 (3.92); 597 (3.77), 652 nm (4.44); HRMS (MALDI) *m/z* calcd. for $C_{52}H_{40}N_4O_{12}$ $[M]^+$: 912.2643, found 912.2650.

Synthesis of 5,10,15,20-Tetrakis[3-(prop-2-yn-1yloxy)phenyl]chlorin (4). *m*-THPC (200 mg, 0.29 mmol.) and K_2CO_3 (406 mg, 2.94 mmol) added to a Schlenk flask. The reagents were dried under vacuum for 1 hour. Dry DMF (10 mL) was added to the flask and the reaction mixture was stirred for 15 minutes. Next, propargyl bromide (349 mg, 2.94 mmol.) was added and the reaction mixture was stirred for 20 hours under an argon atmosphere. The reaction was monitored by TLC. When full conversion of the starting material was observed, the reaction was terminated by the addition of CH_2Cl_2 (50 mL). The reaction mixture was washed using distilled water (2×30 mL), $NaHCO_3$ (2×30 mL), NaCl (2×30 mL) and distilled water (2×30 mL). The organic phase was evaporated under reduced pressure. The product was purified on silica gel column using CH_2Cl_2/n-hexane/methanol (3:1:0.1) as the eluent. The first purple band collected was evaporated under reduced pressure and recrystallized (CH_2Cl_2:hexane). The product was isolated as a purple solid (225 mg, 0.27 mmol, 92%). ^{1}H NMR (400 MHz, chloroform-*d*) δ 8.63 (d, *J* = 4.8 Hz, 2H, H_β), 8.47 (s, 2H, H_β), 8.24 (d, *J* = 4.9 Hz, 2H, H_β), 7.76 (m, 4H, Ar–H), 7.61 (m, 4H, Ar–H), 7.52 (m, 4H, Ar–H), 7.35 (dd, *J* = 8.3, 2.5 Hz, 2H, H_β), 7.29 (dd, *J* = 8.3, 2.5 Hz, 2H, H_β), 4.85 (m, 8H, CH_2), 4.27–4.11 (s, 4H, H_β), 2.57 (s, 4H, alkyne-*H*), −1.48 (s, 2H, N–H) ppm; HRMS (MALDI) *m/z* calc. for $C_{56}H_{40}N_4O_4$ $[M]^+$: 832.3050, found: 832.3040.

Synthesis of 5,10,15,20-Tetrakis[3′-(4′′-ethynylbenzaldehyde)phenoxy]-chlorin (5). A Sonogashira coupling was performed under dry conditions. The *m*-THPC derivative **4** (100 mg, 0.12 mmol.) and 4-iodobenzaldehyde (278 mg, 1.2 mmol) were weighted out and added to a Schlenk flask and dried for 1 hour under vacuum. Next, the compounds were dissolved in dry THF (6 mL) and TEA (3 mL) and stirred for 1 hour. Next, CuI (6.8 mg, 0.036 mmol) and $PdCl_2(PPh_3)_2$ (12 mg, 0.018 mmol) were added. The reaction was monitored by TLC. When full conversion of the starting material was observed, the reaction was terminated, filtered through celite and the crude product was purified on silica gel column (CH_2Cl_2:hexane:methanol – 3:1:0.1). Fraction of TEA (5 mL) was added to neutralize the silica and to reduce stacking of the compound. The first dark-red band collected was evaporated under reduced pressure and recrystallized. The product was isolated as a dark-red solid (67 mg, 0.053 mmol, 45%). M.p.: > 300 °C; R_f = 0.7 (SiO_2, DCM:hexane:MeOH – 3:1:0.1); ^{1}H NMR (400 MHz, chloroform-*d*) δ 10.08–9.88 (s, 4H, CHO), 8.56 (d, *J* = 4.8 Hz, 2H, H_β), 8.41 (s, *J* = 3.3 Hz, 2H, H_β), 8.16 (d, *J* = 3.9 Hz, 2H, H_β), 7.93–7.78 (m, 4H, Ar–H), 7.71 (m, 8H, Ar–H), 7.67–7.61 (m, 4H, Ar–H), 7.60–7.51 (m, 4H, Ar–H), 7.50 (m, 8H, Ar–H), 7.41 (dd, *J* = 8.2, 1.9 Hz, 2H, Ar–H),

7.35 (dd, $J=8.2$, 1.8 Hz, 2H, Ar–H), 5.09 (m, 8H, CH_2), 4.23–3.98 (s, 4H, H_β), −1.49 (s, 2H, N–H) ppm, ^{13}C NMR (101 MHz, chloroform-*d*) δ 191.40, 167.22, 157.09, 155.94, 143.28, 135.77, 132.44, 132.35, 129.45, 129.40, 129.25, 128.35, 127.86, 125.82, 123.53, 118.88, 87.99, 86.59, 56.59, 35.64 ppm; UV/Vis (chloroform): λ_{max} (log ε) = 423 (5.51), 521 (4.37), 548 (4.2), 600 (3.97), 654 nm (4.74); HRMS (MALDI) *m/z* calc. for $C_{84}H_{56}N_4O_8$ $[M]^+$: 1248.4098, found 1248.4124.

Fluorescence decay times and radiative and non-radiative constants

The photoluminescence decay profiles of *m*-THPC and tetrafunctionalized derivatives PS **1**, **3** and **5** were measured through a conventional time correlated single-photon counting (TCSPC) setup, containing a BDL-375-SMN Picosecond Laser Diode (20 MHz, 377 nm), an Acton SpectraPro SP-2300 monochromator (Princeton Instruments), and a high-speed hybrid detector HPM-100–50 (Becker&Hickl GmbH) which was controlled by a DCC-100 card. The fluorescence lifetime values were calculated, after deconvolution procedure of the instrument response function (IRF).

Fluorescence quantum yields

The absolute fluorescence quantum yields (FLQYs) were determined using a FLS 980 Edinburgh Instruments spectrometer, equipped with an integrating sphere and a BDL-375-SMN Picosecond Laser Diode (20 MHz, 377 nm) as an excitation source. Compounds were dissolved in DMF to obtain 10 μM concentration, the sample in a 1 cm quartz cuvette was placed into the center of the integrating sphere. Absolute quantum yield was calculated based on Equation (1):

$$\Phi = \frac{E_b}{S_a - S_b} \quad (1)$$

Where E_b is the integrated fluorescence intensity of the PS sample (600–750 nm), S_a is the integrated excitation peak without presence of the PS (360–400 nm), and S_b is the integrated excitation peak with presence of the PS (360–400 nm).

Average fluorescence lifetimes

In the case of bi-exponential fluorescence decay of PS **5**, the intensity-weighted average value was calculated according to Equation (2):

$$\langle \tau \rangle = \frac{\sum A_i \bullet \tau_i^2}{\sum A_i \bullet \tau_i} \quad (2)$$

Where \[τ\] is the intensity-weighted average fluorescence lifetime (ns), A_i refers to amplitudes (%), and τ_i is fluorescence lifetime components (ns).

For PSs showing mono-exponential fluorescence decay, there is only one fluorescence lifetime component.

Singlet oxygen generation of PSs (direct and indirect method)

The efficiency of singlet oxygen production was studied following the procedure previously described by Silva *et al.*[59] Briefly, $^1O_2$ phosphorescence was detected at 1270 nm at room temperature using a Hamamatsu R5509-42 photomultiplier (cooled with liquid nitrogen) after exciting the solutions of PSs using the second harmonic (532 nm) of a Nd:YAG pulsed laser (8 ns) Spectra-Physics model Quanta-Ray. In order to avoid scattered and fluorescence light Newport long pass filter 10LWF-1000-B were used before the photomultiplier. Solutions of *m*-THPC and tetrafunctionalized derivatives (PS **1**, **3**, and **5**) were prepared in DMSO and DMF obtaining absorbance in a range of ~0.15–0.2 at 532 nm. Rose Bengal was used as a reference; the $^1O_2$ quantum yield for this dye is 0.47 and 0.16 in DMSO and DMF, respectively.[60,61] The $^1O_2$ phosphorescence decay was fitted using a monoexponential function. Pre-exponential factors I_0 were obtained selecting the same time interval for all compounds, then these intensities were plotted in function of the laser pulse energy. The $^1O_2$ quantum yield $\Phi_{eq.}$ was determined using the slope, $m_{\Delta,}$ obtained from the linear fitting of I_0 *in* function of the laser pulse energy [Equation (3)]. Two independent measurements were performed and the average Φ_Δ was calculated for *m*-THPC and tetrafunctionalized derivatives PS **1**, **3** and **5**.

$$\Phi\Delta_x = \frac{\left(1-10^{-A_{ref}}\right)}{\left(1-10^{-A_x}\right)} * \frac{m_x}{m_{ref}} * \Phi_{ref} \quad (3)$$

For Equation (3), A_{ref} refers to the absorbance of the reference at 532 nm, A_x is the absorbance of the compound × at 532 nm, m_x is the slope of the compound *x*, m_{ref} is the slope of the reference, and Φ_{ref} is the $^1O_2$ quantum yield of the reference.

Two-photon excited emission

TPE emission spectra were recorded on a custom-built experimental setup, consisting of a spectrometer (Shamrock 303i, Andor) equipped with an ultrasensitive camera (iDus camera, Andor). All samples were excited with a Ti:Sapphire Chameleon laser (Coherent Inc.), operating from 800 nm to 1080 nm (the repetition rate 80 MHz and the pulse duration ≈120 fs). In order to minimize undesired re-absorption effects and aggregation processes, the relative molar concentrations were adjusted, so the corresponding absorbance values were kept below 0.1 in the emission region. Photostability of each compound was monitored throughout the experiments via absorption and OPE fluorescence measurements. All spectroscopic measurements were performed at room temperature.

Power-dependence measurements

TPE fluorescence spectra of *m*-THPC with the varying laser excitation power (from 2.5 mW to 40 mW) were recorded. The logarithmic emission intensity and laser power values were plotted and then fitted with a linear function.

Two-photon absorption cross-section values

TPA cross-section values were calculated from the TPE emission measurements with the respect to **LDS 698** in chloroform,[53] following Equation (4):

$$\sigma_{TPA,\ sam}[GM] = \sigma_{TPA,\ ref} \frac{I_{sam} C_{ref} n_{ref}^2 \Phi_{ref}}{I_{ref} C_{sam} n_{sam}^2 \Phi_{sam}} \quad (4)$$

where *I* is the integrated emission intensity, *C* is the molar concentration, φ is the OPE fluorescence quantum yield, and *n* is the refractive index of solvent (*sam* refers to sample and *ref* to reference).[62,63,64] The normalized σ_2 values were estimated, follow-

ing Equation (5), where M denotes the molecular weight of the compounds.

$$\sigma_{norm.TPA,sam}[GM/M] = \sigma_{2PA,sam}/M \quad (5)$$

Brightness values were also determined as the multiplication of TPA cross-sections and FLQYs.

Acknowledgements

This work was supported by the Technical University of Munich – Institute for Advanced Study through a Hans Fischer Senior Fellowship (M.O.S.). This work has received funding from the European Union's Horizon 2020 research and innovation programme under the Marie Skłodowska-Curie Grant Agreement No. 764837, the NCN under Opus UMO-2019/35/B/ST4/03280 Grant Agreement, from Science Foundation Ireland (IvP 13/IA/1894) and was supported by the Higher Education Authority and the Department of Further and Higher Education, Research, Innovation and Science (Ireland). We thank Dr. Fábio A. Schaberle (University of Coimbra) and Krzysztof Nadolski (Wroclaw University of Science and Technology) for their guidance and explanation of measurements regarding $^1O_2$ generation efficiency. Open Access funding enabled and organized by Projekt DEAL.

Conflict of Interest

The authors declare no conflict of interest.

Data Availability Statement

The data that support the findings of this study are available from the corresponding author upon reasonable request.

Keywords: nonlinear optics · photodynamic therapy · photosensitizers · porphyrinoids · two-photon absorption

[1] T. J. Dougherty, C. J. Gomer, B. W. Henderson, G. Jori, D. Kessel, M. Korbelik, J. Moan, Q. Peng, *J. Natl. Cancer Inst.* **1998**, *90*, 889–905.
[2] D. van Straten, V. Mashayekhi, H. S. de Bruijn, S. Oliveira, D. J. Robinson, *Cancers* **2017**, *9*, 19.
[3] K. Plaetzer, B. Krammer, J. Berlanda, F. Berr, T. Kiesslich, *Laser Sci. Technol. Second Ser.* **2009**, *24*, 259–268.
[4] Z. Melissari, R. M. Williams, M. O. Senge, in: *Applications of Porphyrinoids as Functional Materials*; Eds. H. Lang; T. Rueffer, Royal Society of Chemistry, Germany, **2021**; pp 252–291.
[5] M. Rumi, J. W. Perry, *Adv. Opt. Photonics* **2010**, *2*, 451–518.
[6] S. Callaghan, M. O. Senge, *Photochem. Photobiol. Sci.* **2018**, *17*, 1490–1514.
[7] L. Luo, Q. Zhang, Y. Luo, Z. He, X. Tian, G. Battaglia, *J. Controlled Release* **2019**, *298*, 99–109.
[8] B. Khurana, P. Gierlich, A. Meindl, L. C. Gomes-da-Silva, M. O. Senge, *Photochem. Photobiol. Sci.* **2019**, *18*, 2613–2656.
[9] S. G. Mucha, L. Firlej, J.-L. Bantignies, A. Żak, M. Samoć, K. Matczyszyn, *RSC Adv.* **2020**, *10*, 38437–38445.
[10] I. Maliszewska, E. Wanarska, A. C. Thompson, I. D. W. Samuel, K. Matczyszyn, *Molecules* **2021**, *26*, 623.
[11] I. Maliszewska, B. Lisiak, K. Popko, K. Matczyszyn, *Photochem. Photobiol.* **2017**, *93*, 1081–1090.
[12] I. Maliszewska, A. Leśniewska, J. Olesiak-Bańska, K. Matczyszyn, M. Samoć, *J. Nanopart. Res.* **2014**, *16*, 2457.
[13] I. S. Mfouo-Tynga, L. D. Dias, N. M. Inada, C. Kurachi, *Photodiagn. Photodyn. Ther.* **2021**, *34*, 102091.
[14] M. Pawlicki, H. A. Collins, R. G. Denning, H. L. Anderson, *Angew. Chem. Int. Ed.* **2009**, *48*, 3244–3266; *Angew. Chem.* **2009**, *121*, 3292–3316.
[15] Z. Sun, L.-P. Zhang, F. Wu, Y. Zhao, *Adv. Funct. Mater.* **2017**, *27*, 1704079.
[16] L. Xu, J. Zhang, L. Yin, X. Long, W. Zhang, Q. Zhang, *J. Mater. Chem. C* **2020**, *8*, 6342–6349.
[17] M. Drobizhev, Y. Stepanenko, Y. Dzenis, A. Karotki, A. Rebane, P. N. Taylor, H. L. Anderson, *J. Am. Chem. Soc.* **2004**, *126*, 15352–15353.
[18] L. M. Mazur, T. Roland, S. Leroy-Lhez, V. Sol, M. Samoć, I. D. W. Samuel, K. Matczyszyn, *J. Phys. Chem. B* **2019**, *123*, 4271–4277.
[19] L. Xu, Q. Zhang, *Sci. China Mater.* **2017**, *60*, 1093–1101.
[20] N. Sheng, D. Liu, J. Wu, B. Gu, Z. Wang, Y. Cui, *Dyes Pigm.* **2015**, *119*, 116–121.
[21] Ò. Rubio-Pons, Y. Luo, H. Ågren, *J. Chem. Phys.* **2006**, *124*, 094310.
[22] Y. Zheng, S. Sun, L. Xu, S. Ni, W. Liu, B. Huang, Q. Huang, Q. Zhang, F. Lu, M.-D. Li, *Dyes Pigm.* **2019**, *165*, 301–307.
[23] M. O. Senge, J. C. Brandt, *Photochem. Photobiol.* **2011**, *87*, 1240–1296.
[24] R. Baskaran, J. Lee, S.-G. Yang, *Biomaterials* **2018**, *22*, 25.
[25] R. Bonnett, R. D. White, U. J. Winfield, M. C. Berenbaum, *Biochem. J.* **1989**, *261*, 277–280.
[26] R. Bonnett, B. D. Djelal, A. Nguyen, *J. Porphyrins Phthalocyanines* **2001**, *5*, 652–661.
[27] L. Rogers, N. N. Sergeeva, E. Paszko, G. M. F. Vaz, M. O. Senge, *PLoS One* **2015**, *10*, e0125372.
[28] L. Rogers, F. Majer, N. N. Sergeeva, E. Paszko, J. F. Gilmer, M. O. Senge, *Bioorg. Med. Chem. Lett.* **2013**, *23*, 2495–2499.
[29] P. Gierlich, A. I. Mata, C. Donohoe, R. M. M. Brito, M. O. Senge, L. C. Gomes-da-Silva, *Molecules* **2020**, *25*, 5317.
[30] E. Gaio, D. Scheglmann, E. Reddi, F. Moret, *J. Photochem. Photobiol. B* **2016**, *161*, 244–252.
[31] M. O. Senge, *Photodiagn. Photodyn. Ther.* **2012**, *9*, 170–179.
[32] I. Yakavets, M. Millard, V. Zorin, H.-P. Lassalle, L. Bezdetnaya, *J. Controlled Release* **2019**, *304*, 268–287.
[33] B. Hamed, T. von Haimberger, V. Kozich, A. Wiehe, K. Heyne, *J. Photochem. Photobiol. A* **2014**, *295*, 53–56.
[34] L. Rogers, E. Burke-Murphy, M. O. Senge, *Eur. J. Org. Chem.* **2014**, *2014*, 4283–4294.
[35] R. Bonnett, B. D. Djelal, G. E. Hawkes, P. Haycock, F. Pont, *J. Chem. Soc., Perkin Trans. 2* **1994**, 1839–1843.
[36] D. M. Fiedler, F. Wierrani, G. Schnitzhofer, J. C. M. Stewart, K. Gharehbaghi, W. Grünberger, B. Krammer, *J. Photochem. Photobiol. B* **1997**, *38*, 241–244.
[37] W. I. White, in: *The Porphyrins*; Ed. D. Dolphin, Elsevier, Canada, **2012**, *Vol. 5*, pp. 303–335.
[38] R. Bonnett, P. Charlesworth, B. D. Djelal, S. Foley, D. J. McGarvey, T. G. Truscott, *J. Chem. Soc., Perkin Trans. 2* **1999**, 325–328.
[39] P. R. Ogilby, C. S. Foote, *J. Am. Chem. Soc.* **1983**, *105*, 3423–3430.
[40] H. Mojzisova, S. Bonneau, P. Maillard, K. Berg, D. Brault, *Photochem. Photobiol. Sci.* **2009**, *8*, 778–787.
[41] Y. Chen, S. Xu, L. Li, M. Zhang, J. Shen, T. Shen, *Dyes Pigm.* **2001**, *51*, 63–69.
[42] B. Aveline, O. Delgado, D. Brault, *J. Chem. Soc. Faraday Trans.* **1992**, *88*, 1971–1976.
[43] P. R. Ogilby, J. Sanetra, *J. Phys. Chem.* **1993**, *97*, 4689–4694.
[44] J. Varchola, K. Želonková, D. Chorvat Jr, D. Jancura, P. Miskovsky, G. Bánó, *J. Lumin.* **2016**, *177*, 17–21.
[45] A. Staicu, A. Pascu, M. Boni, M. L. Pascu, M. Enescu, *J. Mol. Struct.* **2013**, *1044*, 188–193.
[46] M. Hajimohammadi, N. Safari, H. Mofakham, A. Shaabani, *Tetrahedron Lett.* **2010**, *51*, 4061–4065.
[47] S. Oelckers, T. Hanke, B. Röder, *J. Photochem. Photobiol. A* **2000**, *132*, 29–32.
[48] D. Wawrzyńczyk, *J. Mater. Chem. C* **2017**, *5*, 1724–1729.
[49] S. H. Yau, N. Abeyasinghe, M. Orr, L. Upton, O. Varnavski, J. H. Werner, H.-C. Yeh, J. Sharma, A. P. Shreve, J. S. Martinez, T. Goodson III, *Nanoscale* **2012**, *4*, 4247–4254.
[50] J. Arnbjerg, A. Jiménez-Banzo, M. J. Paterson, S. Nonell, J. I. Borrell, O. Christiansen, P. R. Ogilby, *J. Am. Chem. Soc.* **2007**, *129*, 5188–5199.

[51] M. Atif, P. E. Dyer, T. A. Paget, H. V. Snelling, M. R. Stringer, *Photodiagn. Photodyn. Ther.* **2007**, *4*, 106–111.
[52] M. Schneider, G. Graschew, T. A. Roelofs, E. Balanos, S. Rakowsky, H. Sinn, P. M. Schlag, *Proc. SPIE Optical Methods for Tumor Treatment and Detection: Mechanisms and Techniques in Photodynamic Therapy IX* **2000**, *3909*, 60–65.
[53] N. S. Makarov, J. Campo, J. M. Hales, J. W. Perry, *Opt. Mater. Express* **2011**, *1*, 551–563.
[54] Z. Long, J. Wu, S. Yang, Z. Deng, Y. Zheng, W. Zhang, X.-F. Jiang, F. Lu, M.-D. Li, L. Xu, *J. Mater. Chem. C* **2021**, *9*, 11679–11689.
[55] C.-K. Wang, P. Macak, Y. Luo, H. Ågren, *J. Chem. Phys.* **2001**, *114*, 9813–9820.
[56] O. Mongin, V. Hugues, M. Blanchard-Desce, A. Mehri, S. Drouet, D. Yao, C. Paul-Roth, *Chem. Phys. Lett.* **2015**, *625*, 151–156.
[57] S. Sumalekshmy, M. M. Henary, N. Siegel, P. V. Lawson, Y. Wu, K. Schmidt, J.-L. Brédas, J. W. Perry, C. J. Fahrni, *J. Am. Chem. Soc.* **2007**, *129*, 11888–11889.
[58] E. Robbins, S. Leroy-Lhez, N. Villandier, M. Samoć, K. Matczyszyn, *Molecules* **2021**, *26*, 6323.
[59] E. F. F. Silva, F. A. Schaberle, C. J. P. Monteiro, J. M. Dąbrowski, L. G. Arnaut, *Photochem. Photobiol. Sci.* **2013**, *12*, 1187–1192.
[60] D. Wöhrle, M. Shopova, S. Müller, A. D. Milev, V. N. Mantareva, K. K. Krastev, *J. Photochem. Photobiol. B* **1993**, *21*, 155–165.
[61] U. Michelsen, G. Schnurpfeil, A. K. Sobbi, D. Wöhrle, H. Kliesch, *Photochem. Photobiol.* **1996**, *64*, 694–701.
[62] R. Medishetty, J. K. Zaręba, D. Mayer, M. Samoć, R. A. Fischer, *Chem. Soc. Rev.* **2017**, *46*, 4976–5004.
[63] M. Samoć, K. Matczyszyn, M. Nyk, J. Olesiak-Bańska, D. Wawrzyńczyk, P. Hanczyc, J. Szeremeta, M. Wielgus, M. Gordel, L. Mazur, R. Kolkowski, B. Straszak, M. P. Cifuentes, M. G. Humphrey, *Proc. SPIE Organic Photonic Materials and Devices XIV* **2012**, *8258*, 82580 V.
[64] R. L. Roberts, T. Schwich, T. C. Corkery, M. P. Cifuentes, K. A. Green, J. D. Farmer, P. J. Low, T. B. Marder, M. Samoć, M. G. Humphrey, *Adv. Mater.* **2009**, *21*, 2318–2322.

Manuscript received: October 21, 2021
Revised manuscript received: November 30, 2021
Accepted manuscript online: December 9, 2021
Version of record online: January 10, 2022